

Improved estimates of the pion-photon transition form factor in the $(1 \leq Q^2 \leq 5) \text{ GeV}^2$ range and their theoretical uncertainties

S. V. Mikhailov^{1,a}, A. V. Pimikov^{1,2,b}, and N. G. Stefanis^{3,c}

¹*Bogoliubov Laboratory of Theoretical Physics, JINR, 141980 Dubna, Russia*

²*Institute of Modern Physics, Chinese Academy of Sciences, Lanzhou, 730000, P. R. China*

³*Institut für Theoretische Physik II, Ruhr-Universität Bochum, D-44780 Bochum, Germany*

Abstract. We consider the pion-photon transition form factor at low to intermediate spacelike momenta within the theoretical framework of light-cone sum rules. We derive predictions which take into account all currently known contributions stemming from QCD perturbation theory up to the next-to-next-to-leading order (NNLO) and by including all twist terms up to order six. In order to enable a more detailed comparison with forthcoming high-precision data, we also estimate the main systematic theoretical uncertainties, stemming from various sources, and discuss their influence on the calculations — in particular the dominant one related to the still uncalculated part of the NNLO contribution. The analysis addresses, in broad terms, also the role of the twist-two pion distribution amplitude derived with different approaches.

1 Introduction

Collinear factorization [1–4] provides a firm foundation for the application of Quantum Chromodynamics (QCD) to the hard exclusive reactions of hadrons. This makes it possible to calculate partonic subprocesses in a controllable way within QCD perturbation theory. In addition, one needs a reliable framework to include higher twist contributions which represent nonperturbative power corrections. The binding effects ensuing from the confining quark-gluon dynamics are factorized out and have to be determined by other means, e.g., from experiment, lattice simulations, or nonperturbative models.

Consider, for example, the process $\gamma^*(q_1^2)\gamma^*(q_2^2) \rightarrow \pi^0$, with $q_1^2 = -Q^2$ and $q_2^2 = -q^2$. Here the leading-twist two transition form factor (TFF) for two highly off-shell photons can be written in factorized form at the momentum scale μ_F^2 in the form [5]

$$F^{\gamma^*\gamma^*\pi^0}(Q^2, q^2; \mu_F^2) = T(Q^2, q^2; \mu_F^2; x) \otimes \varphi_\pi^{(2)}(x, \mu_F^2), \quad (1)$$

where $\varphi_\pi^{(2)}(x, \mu_F^2)$ is the pion distribution amplitude (DA) of leading-twist two and $\otimes \equiv \int_0^1 dx$. The pion DA has a nonperturbative origin and interpolates between the partonic degrees of freedom of

^ae-mail: mikhs@theor.jinr.ru

^be-mail: pimikov@mail.ru

^ce-mail: stefanis@tp2.ruhr-uni-bochum.de

QCD (quarks and gluons) and the pion bound state

$$\langle 0 | \bar{q}(z) \gamma_\mu \gamma_5 [z, 0] q(0) | \pi(P) \rangle|_{z^2=0} = i f_\pi P_\mu \int_0^1 dx e^{ix(z \cdot P)} \varphi_\pi^{(2)}(x, \mu_F^2), \quad (2)$$

where we have employed the lightcone gauge $A^+ = 0$ in order to reduce the gauge link $[z, 0] = \mathcal{P} \exp \left[-ig \int_0^{\infty} dy_\mu A_a^\mu(y) t_a \right]$ to unity. The DA $\varphi_\pi^{(2)}(x, \mu^2)$ describes the partition of longitudinal-momentum fractions between the valence quark ($x_q = x = (k^0 + k^3)/(P^0 + P^3) = k^+/P^+$) and the valence antiquark ($x_{\bar{q}} = 1 - x \equiv \bar{x}$) at the reference scale μ subject to the normalization condition $\int_0^1 dx \varphi_\pi^{(2)}(x, \mu^2) = 1$.

The virtue of the collinear factorization is that the hard-scattering amplitude $T(Q^2, q^2; \mu_F^2; x)$ can be cast in the form of a power-series expansion in terms of the running strong coupling $a_s \equiv \alpha_s(\mu_R^2)/4\pi$:

$$T(Q^2, q^2; \mu_F^2; x) = T_{\text{LO}} + a_s T_{\text{NLO}} + a_s^2 T_{\text{NNLO}} + \dots \quad (3)$$

becoming calculable within perturbative QCD. Note that the so-called default scale setting has been adopted, i.e., the renormalization scale μ_R and the factorization scale μ_F have been identified, so that $a_s(\mu_R^2) = a_s(\mu_F^2)$. Moreover, we are using here and below the following convenient abbreviations: LO (leading order), NLO (next-to-leading order), NNLO (next-to-next-to-leading order). These contributions will be denoted in terms of the labels (0), (1), and (2), respectively. The NLO term is completely known [6, 7], whereas the calculation of the NNLO contribution has not been completed yet. As we will discuss later in more detail, the uncalculated part entails the strongest theoretical uncertainty (see [8] for a deeper exploration of this issue).

Adopting particular models for the pion DA, one can safely compute at the leading-twist two level $F^{\gamma^* \gamma^* \pi^0}$ using the above expansion and taking into account the Efremov-Radyushkin-Brodsky-Lepage (ERBL) evolution equation [2–4] in order to connect the result obtained at the initial scale μ_0 to any higher momentum value. However, in real experiments one of the photons is almost real, meaning that its virtuality $q_2^2 \gtrsim 0$ is so small that one needs to include its hadronic large-distance content. As a result, perturbative QCD cannot be reliably applied to the calculation of the $F^{\gamma^* \gamma \pi^0}(Q^2, q^2 \gtrsim 0)$ TFF.

A convenient framework to calculate the TFF for $q^2 \rightarrow 0$, is provided by the method of light-cone sum rules (LCSR), developed in [9, 10], which relies upon local duality in the vector channel in terms of a dispersion relation. The key ingredient of this framework is the spectral density

$$\bar{\rho}(Q^2, x) = (Q^2 + s) \rho^{\text{pert}}(Q^2, s), \quad (4)$$

where

$$\rho^{\text{pert}}(Q^2, s) = \frac{1}{\pi} \text{Im} \left[F_{\text{pert}}^{\gamma^* \gamma^* \pi^0}(Q^2, -s - i\varepsilon) \right] \quad (5)$$

and $s = \bar{x}Q^2/x$. Then, one can express the TFF for one highly virtual and one almost real photon as

$$Q^2 F^{\gamma^* \gamma \pi}(Q^2) = \frac{\sqrt{2}}{3} f_\pi \left[\frac{Q^2}{m_\rho^2} \int_{x_0}^1 \exp\left(\frac{m_\rho^2 - Q^2 \bar{x}/x}{M^2}\right) \bar{\rho}(Q^2, x) \frac{dx}{x} + \int_0^{x_0} \bar{\rho}(Q^2, x) \frac{dx}{\bar{x}} \right], \quad (6)$$

where $x_0 = Q^2/(Q^2 + s_0)$ with $s_0 \simeq 1.5 \text{ GeV}^2$ and M^2 is the (auxiliary) Borel parameter. The LCSR method has been applied to the pion-photon TFF in several papers, see for instance, [7, 8, 10–19].

On the experimental side, there are several sets of data from low Q^2 values up to almost 40 GeV^2 taken at single-tag experiments. The increase of the data above 10 GeV^2 , observed by the *BABAR*

Collaboration [20], has not been confirmed by the more recent measurements of the Belle experiment [21]. In the intermediate range of momenta $[5 - 9] \text{ GeV}^2$, both data sets are compatible with each other and agree with the previous CLEO data [22] but bear smaller statistical errors. Finally, in the low- Q^2 regime below 5 GeV^2 down to 1 GeV^2 one can take recourse only to the CLEO data and the older CELLO data [23] which, however, have rather large uncertainties. The BESIII Collaboration have announced high-precision data around 3 GeV^2 in the next future.¹ For the time being, they have only released simulated data in the interval $Q^2 \in [0.5 - 3] \text{ GeV}^2$ [24]. This “data” set merely serves to effect the expected small size of the experimental errors in the event analysis. This notwithstanding, a higher accuracy and precision of experimental data demands more reliable theoretical predictions and better control of their uncertainties. It is just this issue to which this study is devoted, while for the full-fledged analysis we refer to [8]. In the next section we will expand the above exposition and consider its main ingredients in more technical detail (Sec. 2). Our main results and predictions will be given in Sec. 3 followed by our conclusions in Sec. 4.

2 Theoretical framework

In continuation of the previous considerations, we now focus our attention to the spectral density, starting with its twist decomposition [10]:

$$\rho^{\text{pert}}(Q^2, s) = \rho_{\text{tw-2}} + \rho_{\text{tw-4}} + \rho_{\text{tw-6}} + \dots \quad (7)$$

The next step is to expand the twist-two part $\bar{\rho}(Q^2, x)$ in (6) in terms of the partial spectral densities $\bar{\rho}_n$ which are associated with the eigenfunctions ψ_n of the ERBL evolution equation. The set $\{\psi_n\}$ represents a conformal basis for the expansion of the pion DA which reads

$$\varphi_\pi^{(2)}(x, \mu^2) = \psi_0(x) + \sum_{n=2,4,\dots}^{\infty} a_n(\mu^2) \psi_n(x), \quad (8)$$

where the conformal coefficients a_n encode the nonperturbative properties of the DA, while the lowest-order term of this expansion, $\psi_0(x) = \varphi_\pi^{\text{asy}} = 6x\bar{x}$ represents the asymptotic (asy) DA (dashed-dotted line in Fig. 1).

The sum over partial densities then becomes

$$\bar{\rho}(Q^2, x) = \sum_{n=0,2,4,\dots} a_n(Q^2) \bar{\rho}_n(Q^2, x) + \bar{\rho}_{\text{tw-4}}(Q^2, x) + \bar{\rho}_{\text{tw-6}}(Q^2, x), \quad (9)$$

where

$$\begin{aligned} \bar{\rho}_n(Q^2, x) &= \bar{\rho}_n^{(0)}(x) + a_s \bar{\rho}_n^{(1)}(Q^2, x) + a_s^2 \bar{\rho}_n^{(2)}(Q^2, x) + \dots, \\ \bar{\rho}_n^{(0)}(x) &= \psi_n(x); \quad a_s = a_s(Q^2), \end{aligned} \quad (10)$$

with the explicit expressions for the various terms being given in Appendix B of Ref. [8].

The other two contributions to the spectral density of higher twist comprise the twist-four and the twist-six terms. The twist-four term is given by [10]

$$\bar{\rho}_{\text{tw-4}}(Q^2, x) = \frac{\delta_{\text{tw-4}}^2(Q^2)}{Q^2} x \frac{d}{dx} \varphi_\pi^{(4)}(x), \quad (11)$$

¹A. Denig, this conference.

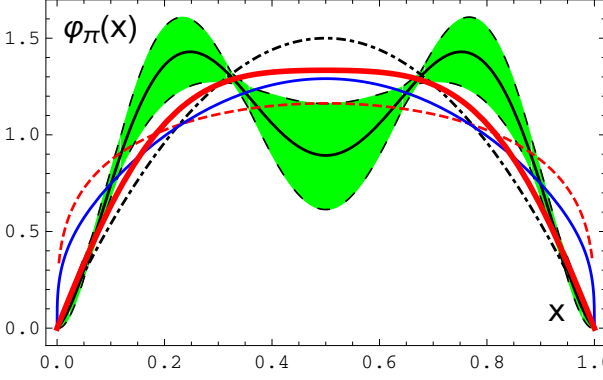


Figure 1. Various pion DAs at the momentum scale $\mu = 2$ GeV. The shaded band in green color displays the bimodal DAs derived in [25] with QCD sum rules which employ nonlocal condensates with a quark virtuality $\lambda_q^2 = 0.4$ GeV². The thick solid red line shows the platykurtic DA, obtained in [26] using the same method but with the value $\lambda_q^2 = 0.45$ GeV². The solid blue line just below it and the broad dashed curve in red represent the results found within the DSE approach [27] — termed DSE-DB and DSE-RL, respectively (see text and Table 1). The dashed-dotted black line is the asymptotic DA.

where the twist-four coupling parameter is defined by $\delta_{\text{tw-4}}^2 \approx (1/2)\lambda_q^2 = (1/2)(0.4 \pm 0.05)$ GeV² at $Q^2 \approx 1$ GeV² [7] and λ_q^2 is the average virtuality of vacuum quarks [28]. In our actual calculations the twist-four pion DA is approximated by its asymptotic form [10, 15]

$$\varphi_\pi^{(4)}(x) = \frac{80}{3}x^2(1-x)^2. \quad (12)$$

The twist-six term in Eq. (9), $\bar{\rho}_{\text{tw-6}}(Q^2, x) = (Q^2 + s)\rho_{\text{tw-6}}(Q^2, s)$, was first computed in [15] and was recently confirmed by an independent calculation in [8]. It can be expressed as follows

$$\bar{\rho}_{\text{tw-6}}(Q^2, x) = 8\pi \frac{C_F}{N_c} \frac{\alpha_s \langle \bar{q}q \rangle^2}{f_\pi^2} \frac{x}{Q^4} \left[-\left[\frac{1}{1-x} \right]_+ + (2\delta(\bar{x}) - 4x) + (3x + 2x \log x + 2x \log \bar{x}) \right] \quad (13)$$

with $\alpha_s = 0.5$, $C_F = 4/3$, $N_c = 3$, and $\langle \bar{q}q \rangle^2 = (0.242 \pm 0.01)^6$ GeV⁶ [29].

The key virtue of the LCSR method relative to the factorization approach of perturbative QCD is that it offers the possibility to include into the TFF the higher eigenfunctions $\psi_{n>0}(x)$ in a successive way in accordance with the increase of the momentum Q^2 . Thus, one can evaluate the TFF

$$Q^2 F^{\gamma^* \gamma \pi^0}(Q^2) = \underbrace{F_0(Q^2) + \sum_n a_n(Q^2) F_n(Q^2)}_{\text{Tw-2}} + F^{(4)}(Q^2) + F^{(6)}(Q^2), \quad (14)$$

where the underbraced terms constitute the leading twist-two contribution, sequentially, i.e., by including with increasing Q^2 more and more terms of the conformal expansion over $\psi_n(x)$. In contrast, the lowest-order leading-twist contribution obtained in perturbative QCD is

$$Q^2 F_n^{\text{pQCD}}(Q^2) = \int_0^1 \psi_n(x) \frac{dx}{\bar{x}} = 3 \quad \text{for } \forall n \quad (15)$$

and therefore all terms of the conformal expansion contribute at once with the effect that $F_n(Q^2)$ does not vary with Q^2 (see [8] for an illustration of this procedure). An important observation is that at low momenta $Q^2 \approx 1$ GeV² mainly the zeroth-order contribution F_0 survives, while the spectral decomposition of the pion DA is less important.

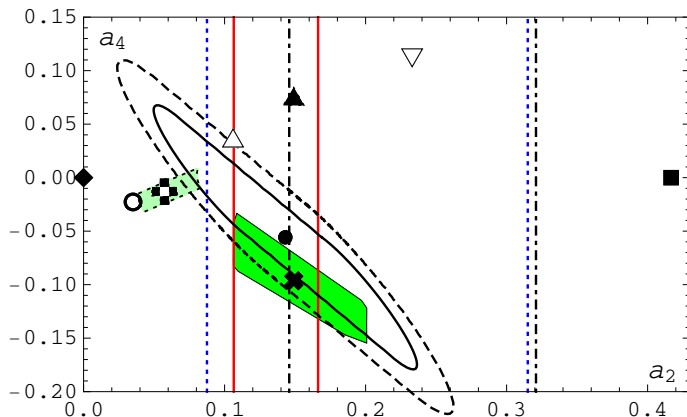


Figure 2. Locations of various pion DAs or of its 2D projections in the space of the conformal coefficients a_2 and a_4 at the scale $\mu = 2$ GeV. The designations are given in Table 1, while theoretical explanations are provided in the text.

Let us now turn our attention to the major nonperturbative input of the TFF, notably, the pion DA. This important quantity is not measurable by itself. Therefore, one has to rely upon its moments

$$\langle \xi^N \rangle_\pi \equiv \int_0^1 \varphi_\pi^{(2)}(x, \mu^2) (x - \bar{x})^N dx, \quad (16)$$

where $\xi = x - \bar{x}$, from which the conformal coefficients a_n in Eq. (8) can be determined (see, for instance, [30, 31] for reviews). For the sake of definiteness, the discussion of the theoretical uncertainties affecting the calculation of the pion-photon TFF is based in our analysis on the pion DAs obtained with the help of QCD sum rules and nonlocal condensates, starting with the paper by the late Bakulev and two of us (Mikhailov and Stefanis) in [25]. This set of DAs, termed BMS, (green band in Fig. 1) was determined by using the mean value of the vacuum quark virtuality $\lambda_q^2 = 0.4$ GeV². All DAs belonging to this set are bimodal distributions with a more or less pronounced dip at $x = 1/2$ and strongly suppressed tails at $x = 0, 1$. Their domain in the parameter space spanned by the Gegenbauer coefficients a_2 and a_4 is shown in the form of a slanted green rectangle in Fig. 2, with the symbol **✕** denoting the BMS model DA. More recently, another DA was derived within the same approach [26, 32, 33], but using the slightly, but still admissible, vacuum quark virtuality $\lambda_q^2 = 0.45$ GeV². This DA is unimodal with a broad peak at $x = 1/2$ but still exhibiting strong suppression of the endpoint regions at $x = 0, 1$, thus giving rise to a platykurtic profile (solid red line in Fig. 1). A dedicated investigation of the endpoint regions of the twist-two pion DA was performed in [34] to which we refer for further reading. Note that arguments for the endpoint suppression of the pion DA were given even earlier [35–37] in the context of quantum fluctuations of the QCD vacuum and the appearance of fermionic zero modes. The graphical representation of the domain of the platykurtic DAs is given by the small slanted rectangle in light-green color in Fig. 2, with the platykurtic DA [26] being denoted by the symbol **♣**. Both types of DAs employ only the first nontrivial coefficients a_2 and a_4 , with the higher ones up to order 10 being determined and found to be close to zero but bearing large uncertainties. Their values were selected to fit best all moments $\langle \xi^N \rangle$ with $N = 2, 4, \dots, 10$ with the mentioned λ_q^2 values [25, 33]. Note that the predictions for the pion-photon TFF computed with the platykurtic DA are very close to the BMS ones [8, 26]. The locations of several other DA models or their 2D

projections have been included in Fig. 2 as well (designations in Table 1). These models are compared with the 1σ and 2σ error ellipses, centered around \bullet , which were obtained by means of LCSRs from the combined analysis of the CELLO [23], CLEO [22], *BABAR* ($\leq 9 \text{ GeV}^2$) [20], and Belle [21] data. The displayed models refer to the scale $Q^2 = 4 \text{ GeV}^2$ after NLO ERBL evolution to that scale, provided the original normalization scale was lower. To complete the picture, also the constraints on a_2 obtained by three different lattice collaborations are also shown in this figure in terms of vertical lines (adding the various errors linearly): solid red lines — $a_2 = 0.1364 \pm 0.0299$ [38]², dashed blue lines — $0.201(114)$ [39], dashed-dotted lines — $0.233(87)$ (result for the larger lattice) [40]. The values of the Gegenbauer coefficients of the pion DAs shown in Fig. 2 are collected in Table 1. We also include the value of the inverse moment $\langle 1/x \rangle_\pi = \int_0^1 dx x^{-1} \varphi_\pi^{(2)}(x) = 3(1 + a_2 + a_4 + \dots) = 3/(\sqrt{2}f_\pi)Q^2 F_{\gamma\pi}^{(2)}(Q^2)$ which gives a crude estimate of the magnitude of the TFF at the Twist-2 level of accuracy. For endpoint-enhanced DAs, this quantity receives additional contributions from the omitted (positive) higher-order coefficients as one sees from the numbers in parentheses which take into account all terms up to a_{12} [41]³.

Table 1. Conformal coefficients a_2 and a_4 , and inverse moment $\langle 1/x \rangle$ at the scale $\mu^2 = 4 \text{ GeV}^2$ related to the pion DAs shown in Fig. 2. NLO evolution is applied if the normalization scale was lower.

Pion DA	a_2	a_4	$\langle 1/x \rangle_\pi$
BMS rectangle [17, 25]	[0.11, 0.20]	[-0.15, -0.03]	[2.88, 3.51]
small slanted green rectangle [33]	[0.04, 0.08]	[-0.03, 0.01]	[3.03, 3.27]
BMS model [8, 25] ✕	$0.149^{+0.052}_{-0.043}$	$-0.096^{+0.063}_{-0.058}$	$3.159^{+0.09}_{-0.09}$
platykurtic model [26, 33] ✚	$0.057^{+0.024}_{-0.019}$	$-0.013^{+0.022}_{-0.019}$	$3.132^{+0.14}_{-0.10}$
center of σ ellipses [17] \bullet	0.143	-0.056	3.261
DSE-DB [27] \blacktriangle	0.149	0.076	3.675 (3.835)
DSE-RL [27] ∇	0.233	0.112	4.035 (4.527)
AdS/QCD [42] \triangle	0.107	0.038	3.435
Light-Front model [43] \circ	0.035	-0.023	3.036
CZ model [30] \blacksquare	0.412	0	4.236
asymptotic \blacklozenge	0	0	3

3 Results and predictions

The theoretical scheme described in the previous section can now be used to derive predictions for the $F^{\gamma^*\gamma\pi^0}(Q^2)$ TFF from small to large values of the momentum transfer Q^2 . We have presented such predictions before focusing attention to the large- Q^2 regime [17–19]. More recently, we addressed the low-to-middle range $Q^2 \leq 5 \text{ GeV}^2$ motivated by the simulated BESIII-data in this domain [8]. In order to match the promised high statistical accuracy of these data, we attempted i) to improve the knowledge of the theoretical ingredients of the analysis and ii) to estimate more reliably the associated theoretical uncertainties. With regard to the first issue, let us display the various terms entering Eq.

²The subtleties related to the continuum limit in extracting a_2 from $\langle \xi^2 \rangle$ have been discussed in [33].

³All coefficients up to order 40 are positive numbers — P. Tandy, this conference.

(3) for the hard-scattering amplitude T up to the contribution proportional to a_s^2 :

$$T_{\text{LO}} = T_0, \quad (17a)$$

$$T_{\text{NLO}} = C_F T_0 \otimes [\mathcal{T}^{(1)} + L V_+^{(0)}], \quad (17b)$$

$$\begin{aligned} T_{\text{NNLO}} = & C_F T_0 \otimes [\mathcal{T}^{(2)} + L V_+^{(1)}/C_F - L \beta_0 \mathcal{T}^{(1)} \\ & - \frac{L^2}{2} \beta_0 V_+^{(0)} + \frac{L^2}{2} C_F V_+^{(0)} \otimes V_+^{(0)} \\ & + L C_F \mathcal{T}^{(1)} \otimes V_+^{(0)}]. \end{aligned} \quad (17c)$$

Note that here and below the convenient abbreviation [6] $L \equiv \ln[(Q^2 y + q^2 \bar{y})/\mu_F^2]$ is used.

The NLO term T_{NLO} is completely known [6, 7]. Consider now the NNLO term T_{NNLO} which can be cast in the form (see [8])

$$T_{\text{NNLO}} = C_F T_0 \otimes [\beta_0 T_\beta + T_{\Delta V} + T_L + \mathcal{T}_c^{(2)}], \quad (18)$$

where

$$T_{\Delta V} = L \Delta V_+^{(1)}, \quad (19a)$$

$$T_L = C_F L \left(\frac{L}{2} V_+^{(0)} \otimes V_+^{(0)} + \mathcal{T}^{(1)} \otimes V_+^{(0)} \right). \quad (19b)$$

The explicit expressions for the above terms can be found in Appendix A of Ref. [8]. What is worth emphasizing here is that the terms $T_{\Delta V}$ and T_L have been calculated for the first time in [8] and are given there in Appendix B. These two additional terms give a small contribution to the TFF as we will discuss later. Finally, the term $\mathcal{T}_c^{(2)}$ is the remaining term at NNLO which is still unknown. On the nonperturbative side, we recalculated term-by-term in [8] the twist-six correction to the TFF and confirmed the original computation in [15]. These improvements increase the reliability of our theoretical predictions and gives us better control over the uncertainties associated with them.

The main theoretical uncertainties originate from three different sources, which can be ordered according to their twist:

- Tw-2: Variation of the pion DA in terms of the conformal coefficients $a_n(Q^2)$ — custom to the method used.
- Tw-2: Uncalculated NNLO term T_c in the TFF.
- Tw-4: Value of λ_q^2 (related to $\delta_{\text{tw-4}}^2$) entering the calculation of the DAs in the approach with nonlocal condensates and independently also the computation of the TFF via the spectral density $\bar{\rho}_{\text{tw-4}}(Q^2, x)$ in LCSR.
- Tw-6: Value of $\alpha_s \langle \bar{q}q \rangle^2$ parameterizing the spectral density $\bar{\rho}_{\text{tw-6}}(Q^2, x)$.

In addition, there are theoretical uncertainties related to auxiliary parameters employed in the LCSR. These are the Borel parameter M^2 and the parametrization procedure of the $(\omega)\rho$ -meson resonance on the right-hand side of Eq. (6). Finally, the calculated TFF depends on the small virtuality of the quasi-real photon whose value is fixed by each particular experiment. In our work we employ for the estimation of this effect the value $q^2 = 0.04 \text{ GeV}^2$ which is related to the Belle experiment.⁴ The detailed estimates in percentage of all these uncertainties at $Q^2 = 3 \text{ GeV}^2$ were tabulated in [8] using $M^2 \in [0.7 - 1.0] \text{ GeV}^2$ as in [17, 18], but also the value $M^2 = 1.5 \text{ GeV}^2$ employed in [15, 16].

⁴S. Uehara, private communication.

Here, we only illustrate in Fig. 3 the select main theoretical uncertainties by displaying $Q^2 F_{\gamma\pi}(Q^2)$ in the momentum range $\leq 5 \text{ GeV}^2$ for the BMS DA (solid black line) and for the platykurtic one (dashed blue line). The amount of these uncertainties is effected in terms of colored strips, as indicated in the figure. The influence of the variation of the auxiliary quantities, mentioned above, and the impact of a finite virtuality of the quasi-real photon can be found in our encompassing analysis in [8]. Note that the reliability of our theoretical predictions below $\sim 1 \text{ GeV}^2$ becomes insufficient.

Some more comments are here in order. Our comparison in Fig. 2 also includes the (a_2, a_4) projections of the two broad unimodal pion DAs obtained from Dyson-Schwinger equations (DSE) [27]. The DA termed DSE-RL was derived by using the rainbow-ladder truncation (symbol ∇), while its more advanced version — coined DSE-DB — employs the most improved kernel to express Dynamical Chiral Symmetry Breaking (DCSB) (symbol \blacktriangle) — called “DB truncation”. As one sees from Table 1, the DSE-DB π DA leads at $\mu^2 = 4 \text{ GeV}^2$ to the same a_2 value 0.149 as the BMS DA. This value is supported by the latest lattice simulation in [38] but is, in contrast to the BMS DA, outside the 1σ (solid line) and 2σ (dashed line) error ellipses obtained with a LCSR-fit to the CELLO, CLEO, *BABAR* ($\leq 9 \text{ GeV}^2$), and Belle data (see Fig. 2) because a_4 is sizeable and positive. Remarkably, the authors of [41] obtain with the DSE-DB pion DA a TFF prediction within their framework which agrees well with all these data and thus belongs to the green band of predictions described in [18]. Last but not least: the similarly broad DA $(8/\pi) \sqrt{x\bar{x}}$, based on the AdS/QCD and light-front holography [42] (its 2D projection is denoted by the symbol \triangle in Fig. 2) turns out to be just inside the 2σ error ellipse of the above sets of experimental data yielding a TFF prediction [42, 44] which belongs to the green band in [18] as well.

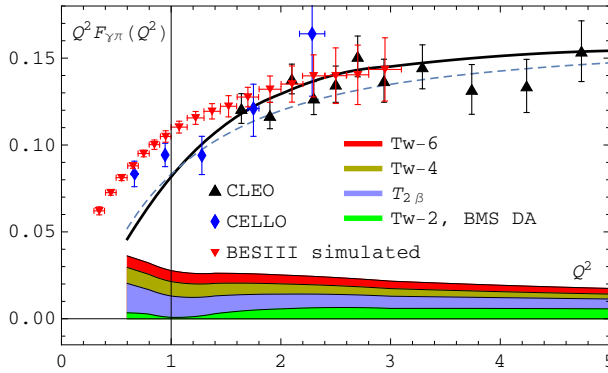


Figure 3. Predictions for the pion-photon TFF within our LCSR method at low- Q^2 in comparison with the existing data of CELLO [23] and CLEO [22], and the simulated data of BESIII [24]. The solid black line shows the result for the BMS DA and the dashed blue line below it the analogous result obtained with the platykurtic DA. Only the key theoretical errors are displayed in the form of colored strips as indicated (see text).

4 Conclusions

In this paper we have described a theoretical approach based on LCSRs to handle the calculation of the pion-photon TFF $F^{\gamma^* \gamma \pi^0}(Q^2)$ including its main theoretical uncertainties which originate from different ingredients of the approach. The key observations pertaining to the reliability of our predictions and the role of the involved uncertainties can be summarized as follows.

- The unknown NNLO term T_c of the radiative corrections generates the largest uncertainty.
- Most of the theoretical uncertainties are correlated at different values of Q^2 .
- At low momenta, the TFF is more sensitive to the variations of the higher-twist contributions Tw-4 and Tw-6 and less sensitive to the values of the conformal parameters a_n describing the pion DA. Indeed, in the vicinity of $Q^2 = 1 \text{ GeV}^2$ the sensitivity to a_n disappears completely as one observes from the green strip at the bottom of Fig. 3.
- The platykurtic pion DA yields a TFF prediction close to the result obtained with the original bimodal BMS DA. The common feature of these DAs is the suppression of the endpoints. Both types of DAs yield predictions which agree rather well with the available experimental data in the range $1 \leq Q^2 \leq 5 \text{ GeV}^2$ and also all higher ones compatible with QCD scaling [18, 26].

It is interesting to extend the above discussion a bit further and mention that also the DA determined in Ref. [43] within a light-front quark model has a platykurtic shape (symbol \bigcirc in Fig. 2) and reproduces all data on $F^{\gamma^* \gamma \pi^0}(Q^2)$, i.e., belongs to the green band of predictions in the classification scheme of [18]. In the same context we note that a recent simultaneous analysis of the CLEO [22] and Belle [21] data in Ref. [45] favors a platykurtic DA profile as well — see [33] for a more detailed comparison. Moreover, a brand-new analysis of the TFF finds best agreement with all sets of existing data except those of *BABAR* above 10 GeV^2 using a spin-improved holographic pion twist-two DA with platykurtic profile [46].

We look ahead for the high-precision data by the BESIII Collaboration in the near future and the high- Q^2 data on two-photon physics to be measured by the BelleII experiment at the end of this decade.

Acknowledgements

This work was partially supported by the Heisenberg–Landau Program (Grant 2016), and the Russian Foundation for Basic Research under Grants No. 14-01-00647, No. 15-52-04023. A.P. has been supported by the “Chinese Academy of Sciences President’s International Fellowship Initiative” under Grant No. 2016PM053, and NSFC Grants No. 11650110431 and No. 11575254.

References

- [1] A.V. Efremov, A.V. Radyushkin, Phys. Lett. **B94**, 245 (1980)
- [2] A.V. Efremov, A.V. Radyushkin, Theor. Math. Phys. **42**, 97 (1980)
- [3] G.P. Lepage, S.J. Brodsky, Phys. Lett. **B87**, 359 (1979)
- [4] G.P. Lepage, S.J. Brodsky, Phys. Rev. **D22**, 2157 (1980)
- [5] S.J. Brodsky, G.P. Lepage, Phys. Rev. **D24**, 1808 (1981)
- [6] B. Melić, D. Müller, K. Passek-Kumerički, Phys. Rev. **D68**, 014013 (2003), hep-ph/0212346
- [7] A.P. Bakulev, S.V. Mikhailov, N.G. Stefanis, Phys. Rev. **D67**, 074012 (2003), hep-ph/0212250
- [8] S.V. Mikhailov, A.V. Pimikov, N.G. Stefanis, Phys. Rev. **D93**, 114018 (2016), 1604.06391
- [9] I.I. Balitsky, V.M. Braun, A.V. Kolesnichenko, Nucl. Phys. **B312**, 509 (1989)
- [10] A. Khodjamirian, Eur. Phys. J. **C6**, 477 (1999), hep-ph/9712451
- [11] A. Schmedding, O.I. Yakovlev, Phys. Rev. **D62**, 116002 (2000), hep-ph/9905392
- [12] A.P. Bakulev, S.V. Mikhailov, N.G. Stefanis, Phys. Lett. **B578**, 91 (2004), hep-ph/0303039
- [13] A.P. Bakulev, S.V. Mikhailov, N.G. Stefanis, Phys. Rev. **D73**, 056002 (2006), hep-ph/0512119
- [14] S.V. Mikhailov, N.G. Stefanis, Nucl. Phys. **B821**, 291 (2009), 0905.4004

- [15] S.S. Agaev, V.M. Braun, N. Offen, F.A. Porkert, Phys. Rev. **D83**, 054020 (2011), 1012.4671
- [16] S.S. Agaev, V.M. Braun, N. Offen, F.A. Porkert, Phys. Rev. **D86**, 077504 (2012), 1206.3968
- [17] A.P. Bakulev, S.V. Mikhailov, A.V. Pimikov, N.G. Stefanis, Phys. Rev. **D84**, 034014 (2011), 1105.2753
- [18] A.P. Bakulev, S.V. Mikhailov, A.V. Pimikov, N.G. Stefanis, Phys. Rev. **D86**, 031501 (2012), 1205.3770
- [19] N.G. Stefanis, A.P. Bakulev, S.V. Mikhailov, A.V. Pimikov, Phys. Rev. **D87**, 094025 (2013), 1202.1781
- [20] B. Aubert et al. (BaBar), Phys. Rev. **D80**, 052002 (2009), 0905.4778
- [21] S. Uehara et al. (Belle), Phys. Rev. **D86**, 092007 (2012), 1205.3249
- [22] J. Gronberg et al. (CLEO), Phys. Rev. **D57**, 33 (1998), hep-ex/9707031
- [23] H.J. Behrend et al. (CELLO), Z. Phys. **C49**, 401 (1991)
- [24] A. Denig (BESIII), Nucl. Part. Phys. Proc. **260**, 79 (2015), 1412.2951
- [25] A.P. Bakulev, S.V. Mikhailov, N.G. Stefanis, Phys. Lett. **B508**, 279 (2001), [Erratum: Phys. Lett. B590, 309 (2004)], hep-ph/0103119
- [26] N.G. Stefanis, Phys. Lett. **B738**, 483 (2014), 1405.0959
- [27] L. Chang, I.C. Cloet, J.J. Cobos-Martinez, C.D. Roberts, S.M. Schmidt, P.C. Tandy, Phys. Rev. Lett. **110**, 132001 (2013), 1301.0324
- [28] S.V. Mikhailov, A.V. Radyushkin, JETP Lett. **43**, 712 (1986), [Pisma Zh. Eksp. Teor. Fiz.43,551(1986)]
- [29] P. Gelhausen, A. Khodjamirian, A.A. Pivovarov, D. Rosenthal, Phys. Rev. **D88**, 014015 (2013), [Erratum: Phys. Rev. D91, 099901 (2015)], 1305.5432
- [30] V.L. Chernyak, A.R. Zhitnitsky, Phys. Rept. **112**, 173 (1984)
- [31] N.G. Stefanis, Eur. Phys. J. direct **C7**, 1 (1999), hep-ph/9911375
- [32] N.G. Stefanis, S.V. Mikhailov, A.V. Pimikov, Few Body Syst. **56**, 295 (2015), 1411.0528
- [33] N.G. Stefanis, A.V. Pimikov, Nucl. Phys. **A945**, 248 (2016), 1506.01302
- [34] S.V. Mikhailov, A.V. Pimikov, N.G. Stefanis, Phys. Rev. **D82**, 054020 (2010), 1006.2936
- [35] N.G. Stefanis, W. Schroers, H.C. Kim, Phys. Lett. **B449**, 299 (1999), hep-ph/9807298
- [36] N.G. Stefanis, W. Schroers, H.C. Kim, Eur. Phys. J. **C18**, 137 (2000), hep-ph/0005218
- [37] H.M. Choi, C.R. Ji, Phys. Rev. **D75**, 034019 (2007), hep-ph/0701177
- [38] V.M. Braun, S. Collins, M. Göckeler, P. Pérez-Rubio, A. Schäfer, R.W. Schiel, A. Sternbeck, Phys. Rev. **D92**, 014504 (2015), 1503.03656
- [39] V.M. Braun et al., Phys. Rev. **D74**, 074501 (2006), hep-lat/0606012
- [40] R. Arthur, P.A. Boyle, D. Brömmel, M.A. Donnellan, J.M. Flynn, A. Jüttner, T.D. Rae, C.T.C. Sachrajda, Phys. Rev. **D83**, 074505 (2011), 1011.5906
- [41] K. Raya, L. Chang, A. Bashir, J.J. Cobos-Martinez, L.X. Gutiérrez-Guerrero, C.D. Roberts, P.C. Tandy, Phys. Rev. **D93**, 074017 (2016), 1510.02799
- [42] S.J. Brodsky, F.G. Cao, G.F. de Téramond, Phys. Rev. **D84**, 033001 (2011), 1104.3364
- [43] H.M. Choi, C.R. Ji, Phys. Rev. **D91**, 014018 (2015), 1412.2507
- [44] S.J. Brodsky, F.G. Cao, G.F. de Téramond, Phys. Rev. **D84**, 075012 (2011), 1105.3999
- [45] T. Zhong, X.G. Wu, T. Huang, Eur. Phys. J. **C76**, 390 (2016), 1510.06924
- [46] M. Ahmady, F. Chishtie, R. Sandapen (2016), 1609.07024